Journal of Creativity Student
http://journal.unnes.ac.id/journals/jcs

Performance Analysis of a 1-Slot 1-Pole Orbital Electric Motor with Rotor Variations Using ANSYS Electronics

Bagus Akbar Prihartanto[1]*, Widya Aryadi[2]

[1,2]*Department of Mechanical Engineering, Universitas Negeri Semarang, Indonesia*

*Corresponding Author: bagusakbar1311@students.unnes.ac.id

Abstract
Global warming and rising carbon emissions from the transportation sector have accelerated the development of electric vehicles, making the selection of an appropriate electric motor design essential. This study examines the performance characteristics of a ring-type orbital electric motor with a 1-slot 1-pole configuration by comparing two rotor materials, namely pure permanent magnet (Neodymium NdFe30) and low carbon steel (Steel 1010), in terms of flux linkage, electromagnetic force, and torque. Simulations were conducted using ANSYS Maxwell, a Finite Element Method (FEM)-based tool within ANSYS Electronics, employing a Magnetostatic Solver across a rotor rotation angle range of -50° to 50° with a 1° step. The results show that the low carbon steel rotor produced a higher maximum force and torque than the pure permanent magnet rotor, reaching 362.373 N (217% higher than 114.427 N) and 146.829 Nm (17.5% higher than 124.944 Nm), respectively. For flux linkage, both rotors exhibited similar baseline values but moved in opposite directions as the rotor approached its central position, with the low carbon steel rotor increasing to 1.62377 Wb and the pure permanent magnet rotor decreasing to -0.260653 Wb, resulting in a deviation approximately 64.3% larger for the low carbon steel rotor. Across all three parameters, the low carbon steel rotor exhibited sharper and more concentrated fluctuations, whereas the pure permanent magnet rotor produced smoother, more stable, and evenly distributed responses throughout the tested angular range.

Keywords: *electric vehicles, low carbon steel, permanent magnet, ring-type orbital electric motor, torque*

INTRODUCTION

Global warming has posed significant challenges to the sustainable development of the global community. This issue has prompted many countries undergoing economic improvements to seek development measures utilizing low-carbon emission alternative energy sources. Particularly in urban areas, various aspects of life, such as the housing sector, industrial production, and logistics, are the largest contributors to carbon emissions (Guo et al., 2022). This condition is further exacerbated by the continuous use of fossil fuels, which has caused a steady increase in atmospheric CO_2 concentrations, reaching 400.26 ppm (parts per million) in 2015 (Abas et al., 2015). In Indonesia, the carbon emission problem is becoming increasingly apparent alongside the rapid growth of the transportation sector, marked by an increasing number of motorized vehicles that predominantly still rely on oil and gas fuels (Sofaniadi et al., 2022). Based on Statistics Indonesia (BPS) data, the number of motorized vehicles increased from 126,508,776 units in 2018 to 133,617,012 units in 2019, and 136,137,451 units in 2020, resulting in elevated fuel consumption and CO_2 emissions as the primary causes of the greenhouse effect (Fitrianto, 2023). To address this, battery electric vehicles have begun to be developed as a substitute solution for fossil-fueled vehicles; although oil-fueled vehicles generate substantial mechanical power, their pollution impact on the environment is highly significant. The development of electric cars and motorcycles is considered to hold great potential for significantly reducing pollutant emissions such as CO, NO_x, HC, SO_2, and particulate matter (PM) (Sudjoko, 2021).

The selection of an appropriate type of electric motor is crucial for electric vehicles. Brushless Direct Current (BLDC) motors are considered the best choice in terms of efficiency due to their widespread use across various applications. Compared to DC motors, BLDC motors possess a simpler structure, lighter weight, larger starting torque, precise control, and high dynamic response (Khan-Ngern et al., 2018). Their popularity continues to grow rapidly, with broad applications in the automotive, pumping, and milling industries (Mohanraj et al., 2022), and they have become the most frequently used option for electric vehicles (EVs) owing to their high reliability, high efficiency, and wide speed regulation range (Hashemnia & Asaei, 2008). Nevertheless, BLDC motors have efficiency limitations in generating low torque, resulting from the misalignment of the magnetic field direction between the stator and the rotor (Kuczmann, 2024).

As a follow-up to these issues, this study develops a ring-type orbital electric motor design, which utilizes an axial magnetic flux direction as one of the extensively studied approaches in electric motor design development. Unlike conventional radial motors, orbital motors possess a different flux path direction, enabling a more compact configuration form while simultaneously generating higher torque. These findings align with the results of other studies revealing that appropriate stator coil winding arrangements can improve the performance of axial flux-type BLDC motors (Azizi et al., 2020).

Slot and pole configurations also significantly influence the performance characteristics of electric motors, such as torque ripple, maximum output torque, and power losses; therefore, they need to be compared comprehensively (Liu et al., 2024). For this reason, researchers generally employ the Finite Element Method (FEM) to analyze the performance of PMSMs with various slot-pole combinations (Mei et al., 2023). One example is a study by Kahar et al. (2022) conducted on BLDC motors with three different slot-pole configurations, namely 18-20, 12-10, and 9-8. Using a transient magnetic-based FEM approach, the study demonstrated that a higher number of slots and poles resulted in higher Back Electromotive Force (BEMF) values and generated electromagnetic torque.

ANSYS Maxwell is an FEM-based software package from ANSYS Electronics used to solve electromagnetic field problems utilizing Maxwell's equations. It is widely utilized to understand electrical machines and magnetic field effects across various engineering fields, offering detailed design stages and analysis features that facilitate the resolution of electromagnetic problems, and is increasingly common in high-precision electrical machine analysis alongside the development of high-speed computers (Gecer et al., 2020). ANSYS Maxwell is also equipped with an Optimetrics module that enables optimization calculations based on single or multiple criteria, employing various algorithms including genetic algorithms. Its advantage lies in the optimization process being performed directly based on field calculations through the finite element method, ensuring the results closely approach actual prototype conditions (Pliuhin et al., 2022).

This study aims to examine the performance characteristics of a ring-type orbital electric motor with a 1-slot 1-pole configuration by comparing two rotor material variables, namely pure permanent magnets and low-carbon steel. The investigated aspects encompass three primary output variables: flux linkage distribution, electromagnetic force, and torque. The research outcomes are expected to produce ideal outputs and be widely applicable in the development of electric motors. Although previous studies have analyzed this type of motor, there are several shortcomings that need to be re-examined (Hao et al., 2022; Islam et al., 2022); therefore, the results of this study are expected to provide a more profound understanding of the characteristics of ring-type orbital electric motors, while simultaneously serving as a scientific reference and benchmark for the development of more efficient orbital electric motors for future electric vehicle applications.

METHOD

This study employed a quantitative method with a simulation-based experimental design, wherein numerical and graphical data were collected and systematically analyzed to draw conclusions (Sofwatillah et al., 2024). The research was also comparative, contrasting two ring-type orbital electric motor designs with identical configurations but distinct rotor materials. Simulation parameters were pre-determined to ensure consistent results that could be objectively compared. The comparison focused on force, torque, and flux linkage, illustrating the effectiveness of this approach based on the study results between the two motor designs. The utilization of computer-based simulations in this study provided various benefits, such as saving time and costs during the research process, increasing flexibility in testing various conditions, and mitigating risks that could occur during the implementation phase. Furthermore, simulation supports design evaluation and refinement from the early stages, making the development process more effective and minimizing the potential for technical obstacles and financial losses.

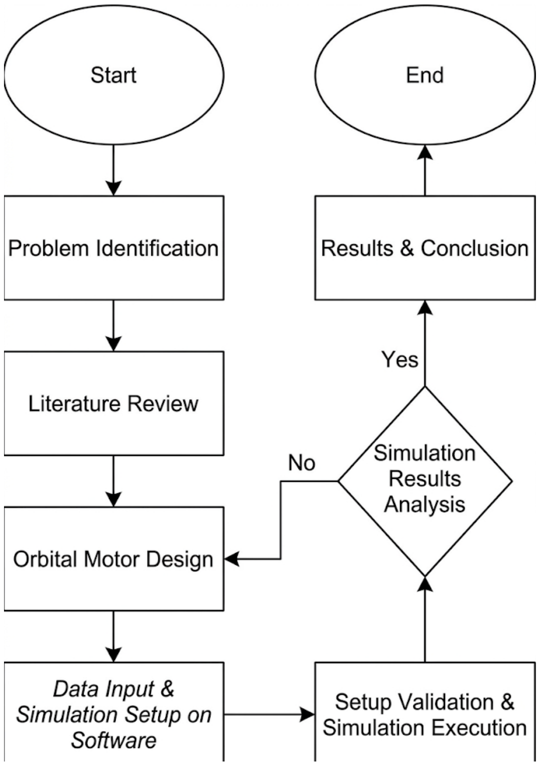

Figure 1. Research Flowchart

The electric motor design utilized in this study refers to a ring-type orbital electric motor, which served as the primary object in the simulation and analysis processes. The design development was conducted with reference to previous studies, encompassing modifications to slot position, slot number, slot dimensions, and rotor material alterations during the simulation process. After all these data were acquired, it was followed by the modeling of the ring-type orbital electric motor using Computer-Aided Design (CAD) software, specifically Autodesk Inventor Professional 2027, to generate a three-dimensional model conforming to the predetermined design specifications. The design specifications of the study are presented in Table 1.

The utilized ring-type orbital electric motor was designed with a 1-slot 1-pole configuration. After the initial modeling and measurement processes were completed, the models were arranged as a three-dimensional assembly using the same software, as depicted in Figure 2. The assembly result or three-dimensional geometry was then saved in a STEP file format. Subsequently, the simulation software was opened, and the solver program was selected to import the file into the simulation and analysis process.

Figure 2. Orbital Motor Assembly Design

Table 1. Motor Geometry Design Specifications

Component	Size	Unit
Rotor Outer Diameter	220	mm
Rotor Inner Diameter	180	mm
Armature Height & Width	95	mm
Stator Height & Width	80	mm
Rotor Thickness	40	mm
Rotor Width	50	mm
Air Gap	0.6	mm

Material selection in this simulation was conducted by considering the physical and mechanical properties of each motor component, ensuring that the utilized material characteristics realistically represented operational conditions. Accuracy in material selection is crucial, given that simulation output magnitudes such as magnetic flux distribution, electromagnetic force, and generated torque are highly influenced by the material characteristics assigned to each motor component. The materials used in this simulation were sourced from the ANSYS software's built-in material library, with details outlined in Table 2.

Table 2. Motor Material Specifications

Component	Material
Armature (Housing)	ABS, Plastic
Stator	Copper
Rotor	Low Carbon Steel 1010, Neodymium NdFe30

The simulation in this study was conducted using ANSYS Maxwell, one of the tools within the ANSYS Electronics software suite, employing a Magnetostatic Solver computational method. Magnetostatic is used to analyze magnetic field conditions that remain constant over time, focusing calculations on inductance, force, and torque among magnetic components (Dermani, 2025). The three-dimensional model that had been created and imported was then utilized as the simulation object to analyze the orbital electric motor's performance based on the designed configuration. ANSYS Maxwell is a high-performance low-frequency electromagnetic field simulation software that utilizes Finite Element Analysis (FEA) methods to solve various electromagnetic problems in two- and three-dimensional electromagnetic and electromechanical devices, such as motors, actuators, transformers, sensors, and coils. The software is also capable of calculating quantities such as force, torque, capacitance, inductance, resistance, and impedance, as well as generating a state-space model (Dusane, 2016).

ANSYS Maxwell resolves electromagnetic field problems by solving Maxwell's equations within a finite region of space, applying user-defined boundary and initial conditions. The simulation domain is discretized (meshing) using triangular (2D) or tetrahedral (3D) elements, with linear interpolation functions to approximate the solution (Dusane, 2016). Maxwell's equations themselves are four fundamental differential equations that describe the relationships among the electric field, electric flux, magnetic field, and magnetic flux density in a medium, considering the sources of charge and electrical current. They serve as the foundation of classical electromagnetic theory used in the analysis and simulation of electromagnetic devices (Jin et al., 2024). The Maxwell method is a numerical method for solving these equations by dividing the domain or complex object into simpler elements (Tjong, 2021).

To analyze the performance characteristics of the orbital electric motor, the simulation within ANSYS Electronics was conducted through a systematic and continuous procedure. The process commenced with the importation of the 3D geometric model and the assignment of specific material properties to the rotor, stator, and housing. Subsequently, winding characteristics and coil terminals were configured based on the number of conductor turns, alongside the designation of target calculation parameters such as force, torque, and flux linkage. The computational environment was then established by defining boundary regions and executing mesh operations utilizing either length-based or skin depth-based criteria. Following the configuration of the solution setup—which detailed the solving method, percent error, and iteration limits—a parametric sweep was applied to incrementally simulate the rotor's rotation angle. Finally, after establishing field overlays (including B Vector, J Vector, and Mag B) and configuring the output reports, a comprehensive validation check was performed to ensure model integrity across all settings prior to executing the simulation via the "analyze all" function and reviewing the generated results.

The input data utilized throughout the simulation process included several primary parameters. These parameters served as the foundation for generating the numerical output data produced by the motor. The input data table used in the simulation is presented in Table 3. To ensure the suitability and accuracy of the motor performance testing, all utilized parameters referred to relevant previous studies (Aryadi et al., 2025). These parameters were then inputted into the winding and coil terminal properties within the simulation software.

Table 3. Simulation Input Data Specification Table

Parameter	Value	Unit
Number of Turns	400	-
Current	46.5	Ampere

The analysis setup and meshing configurations described above function as boundary conditions in the simulation to ensure the obtained results are accurate and consistent. The convergence settings serve to refine the mesh and monitor the numerical accuracy of the solution (Madras Ponnuswamy & Veeranna, 2026). Convergence parameters were set with an error limit of 2% and a refinement per pass of 20% to maintain a balance between accuracy and computational time efficiency. The adaptive pass limits were set with maximum passes at 20, minimum passes at 3, and minimum converged passes at 1 to ensure iteration stability.

During the meshing stage, a length-based mesh operation was applied with a maximum element length set to 1/3 of the geometry, particularly on the rotor and region geometries. The purpose of determining these quantities is to increase mesh density and calculation precision in concentration areas. Determining the number of mesh elements is crucial because it is directly proportional to data reliability and computational duration; the higher the number of elements, the higher the numerical accuracy, although the simulation time becomes longer (Muljono et al., 2025). Furthermore, position evaluation was conducted parametrically using an angle variable (degree) with an initial value of 0° in the Design Properties. The movement testing was configured through a Linear Step-type Setup Sweep Analysis with a degree range starting from -50° to 50° and a step size of 1°, thereby enabling continuous recording of magnetic flux distribution, electromagnetic force, and torque at each incremental rotor position.

RESULTS AND DISCUSSION

The simulation in this study utilized the ANSYS Electronics 2024 software with a three-dimensional (3D) static model approach based on the finite element method (FEA or FEM). The testing was focused on variations in the rotor's degree of shift to evaluate the performance of the ring-type orbital electric motor. Two rotor variations were utilized in this simulation, namely a rotor with pure permanent magnet material and a rotor with low-carbon steel material. This simulation generated three output quantities, namely flux linkage, electromagnetic force, and motor torque, which were reviewed based on changes in the rotor material type and angular position, with the motor configuration remaining at a 1-slot 1-pole configuration throughout all tests. All simulation result data were initially compiled in the form of numerical tables to demonstrate the performance of each rotor and subsequently visualized as line graphs to facilitate the observation of changes resulting from the rotor angle shift. Through these graphs, the patterns and trends of change in each rotor could be seen more clearly, thereby facilitating the drawing of conclusions regarding the effect of the rotor angle on motor performance. The primary objective of this development was to obtain more accurate and optimized simulation results. In this study, the applied differences included rotor angle adjustments and rotor material selection, aiming to evaluate the motor's performance and determine the most efficient rotor configuration. To ensure data consistency, parameters such as the number of turns and input current were aligned with those utilized in previous studies (Choudhary et al., 2019; Ehya et al., 2021).

Based on the graph in Figure 3, both rotors demonstrated that the flux linkage value changed quite significantly alongside the rotor angle shift. The low-carbon steel rotor produced the highest maximum flux linkage, amounting to 1.62377 Wb at an angle of 0°, considerably larger than that of the pure permanent magnet rotor. At both ends of the angular range, the flux linkage values of the low-carbon steel rotor were recorded at 0.456598 Wb at an angle of -50° and 0.456609 Wb at an angle of

50°. The flux linkage value in the low-carbon steel rotor began to rise sharply from an angle of approximately -18°, reached its peak around the 0° angle, and then decreased symmetrically up to the 50° angle, forming a hill-like curve pattern around the rotor's center position.

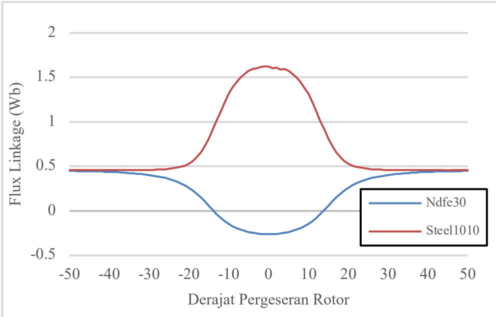

Figure 3. Flux Linkage Output Graph

Conversely, the pure permanent magnet rotor exhibited an opposing pattern, forming a valley-like curve around the rotor's center position. The highest flux linkage values for this rotor were recorded at both ends of the angular range, namely 0.449789 Wb at the -50° angle and 0.449723 Wb at the 50° angle; it then gradually decreased until reaching a peak value of -0.260653 Wb at the 0° angle, before rising symmetrically again toward the other end of the angular range. The decrease in the pure permanent magnet rotor occurred much more gradually compared to the sharp spike in the low-carbon steel rotor. Based on the graph in Figure 4, the force generated by the two rotors exhibited vastly different patterns in response to changes in the rotor angle. The pure permanent magnet rotor tended to be more stable, with relatively small and evenly distributed force fluctuations throughout the entire angular range of -50° to 50°, without any angular sections where the value approached zero and flattened out. The maximum force in this rotor was recorded at 114.427 N at a -15° angle, while the minimum force of -70.418 N occurred at a 10° angle.

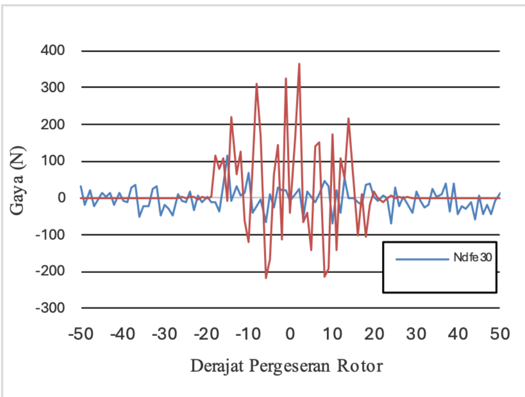

Figure 4. Force Output Graph

In contrast, the low-carbon steel rotor demonstrated a different pattern, where the force value was close to zero and flat at angles outside the -20° to 20° range, but fluctuated sharply and repeatedly upon entering this range. The force fluctuations within this range appeared increasingly larger when approaching the 0° angle, with the most extreme values occurring around the -8° to 8° angles, before diminishing again toward the ±20° angles. The force changes in the low-carbon steel rotor within this range also occurred much more rapidly compared to the pure permanent magnet rotor, marked by numerous changes in the force direction over a short angular distance. This rotor recorded the highest maximum force of 362.373 N at a 2° angle, and a minimum force of -217.457 N at a -6° angle, indicating a much larger fluctuation range compared to the pure permanent magnet rotor within that narrow angular distance. Based on the graph in Figure 5, both rotor configurations displayed torque curves with a sinusoidal pattern, wherein the torque value of each rotor increased alongside the angular shift, and subsequently decreased after passing its peak point. The low-carbon steel rotor produced the highest maximum torque, amounting to 146.829 N·m at a -12° angle, surpassing the pure permanent magnet rotor which reached a maximum torque of 124.944 N·m at a -15° angle. On the flip side, the low-carbon steel rotor also recorded a minimum torque of -146.743 N·m at a 12° angle, while the pure permanent magnet rotor recorded a minimum torque of -124.945 N·m at a 15° angle, demonstrating a symmetrical torque change pattern relative to the 0° angle for both rotor configurations.

In the angular range of -50° to -20°, the torque value of the low-carbon steel rotor remained relatively small, ranging from 0.033 N·m to 32.152 N·m, while the pure permanent magnet rotor in the same angular range exhibited much larger torque values, ranging from -1.401 N·m to -77.700 N·m. However, upon entering the -18° to -12° angular range, the torque of the low-carbon steel rotor increased sharply until it surpassed that of the pure permanent magnet rotor, reaching its peak at the -12° angle with a value of 146.829 N·m, whereas the pure permanent magnet rotor reached its peak slightly later, specifically at the -15° angle. A similar pattern was also observed symmetrically on the positive angle side, where the low-carbon steel rotor again recorded larger extreme values compared to the pure permanent magnet rotor in the angular range of 12° to 18°.

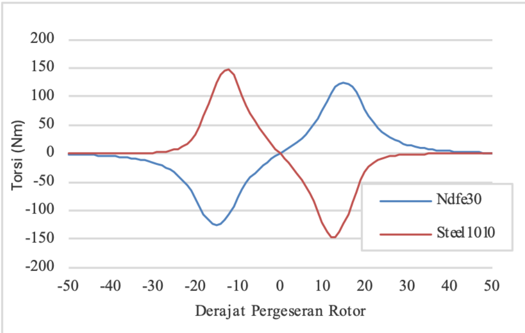

Figure 5. Torque Output Graph

The low-carbon steel rotor generated a larger torque fluctuation range compared to the pure permanent magnet rotor, with a curve that rose and fell more sharply around the -18° to 18° angles, before flattening out again near the initial values at both ends of the angular range. Conversely, the torque curve of the pure permanent magnet rotor exhibited more gradual and smoother changes throughout the tested angular range, without the sharp spikes observed in the low-carbon steel rotor.

CONCLUSION

The simulation in this study utilized ANSYS Electronics 2024 with a 3D static model approach based on the finite element method (FEA or FEM). The testing focused on variations in the rotor angle and material, namely pure permanent magnet and low-carbon steel, to evaluate the performance of a 1-slot 1-pole ring-type orbital electric motor. The simulation generated three output quantities—flux linkage, force, and torque—which were compiled into numerical tables and presented as line graphs. In terms of flux linkage, the values for both rotors were approximately 0.45 Wb at the -50° and 50° angles, which served as reference points due to their relative stability prior to significant shifts caused by changes in the rotor angle. From these reference points, the low-carbon steel rotor experienced an increase, reaching a maximum value of 1.62377 Wb at the 0° angle, representing a rise of 1.1672 Wb, whereas the pure permanent magnet rotor experienced a decrease, reaching a minimum value of -0.260653 Wb at the 0° angle, denoting a drop of 0.7104 Wb (in magnitude). Based on the magnitude of the deviation from the reference point to the extreme point, the low-carbon steel rotor generated a deviation approximately 64.3% larger than that of the pure permanent magnet rotor. The two rotors exhibited opposing curve patterns; the low-carbon steel rotor formed a hill-like curve, whereas the pure permanent magnet rotor formed a valley-like curve, with the extreme points of both located around the 0° angle. Regarding force, the low-carbon steel rotor generated a maximum force of 362.373 N, or approximately 217% higher than the pure permanent magnet rotor, which only reached 114.427 N. The minimum force of the low-carbon steel rotor was also recorded at -217.457 N, or approximately 209% larger in magnitude compared to the pure permanent magnet rotor's minimum force of -70.418 N. The pure permanent magnet rotor demonstrated relatively small and even force fluctuations throughout the angular range, while the low-carbon steel rotor tended to remain flat across most of the range but fluctuated sharply around the middle of the angular shift range. In terms of torque, the low-carbon steel rotor generated a maximum torque of 146.829 N·m, roughly 17.5% higher than the pure permanent magnet rotor's 124.944 N·m. The minimum torque of the low-carbon steel rotor was also recorded at -146.743 N·m, roughly 17.4% larger in magnitude than the pure permanent magnet rotor's minimum torque of -124.945 N·m. Both rotors displayed symmetrical sinusoidal torque curves, with the low-carbon steel rotor exhibiting sharper fluctuations, whereas the pure permanent magnet rotor displayed more gradual and smooth changes. Consequently, the low-carbon steel rotor produced higher peak or maximum values for flux linkage, force, and torque compared to the pure permanent magnet rotor, albeit accompanied by much sharper fluctuations. Conversely, the pure permanent magnet rotor generated lower values but was considerably more stable and uniform throughout the tested angular range. This pattern consistently appeared across all three output graphs.

ACKNOWLEDGMENTS

The author expresses profound gratitude to God Almighty for His abundant grace and blessings, enabling the successful completion of this article. Deepest appreciation is also extended to Universitas Negeri Semarang, particularly the Mechanical Engineering Study Program, for the continuous guidance, facilities, and support. As this research is inseparable from the assistance of various parties, the author expresses the utmost gratitude to Prof. Dr. S. Martono, M.Si., as the Rector of Universitas Negeri Semarang, for the opportunity to pursue these studies, and to Prof. Dr. Wirawan Sumbodo, M.T., as the Dean of the Faculty of Engineering, for his academic and administrative support. Special thanks are directed to Deni Fajar Fitriyana, S.T., M.T., Coordinator of the Mechanical Engineering Study Program, for his continuous encouragement, and to Widya Aryadi, S.T., M.Eng., the academic advisor, for his patient direction and constructive feedback from inception to completion. Furthermore, the author is deeply indebted to their beloved family—their late Father, Mother, and Sibling—for their sincere prayers, sacrifices, and ceaseless moral support. Finally, heartfelt thanks go to the fellow students of the Mechanical Engineering Study Program class of 2022, especially those from the International class, for their camaraderie, motivation, and engaging discussions that have profoundly broadened the author's perspectives and mindset during this educational journey.

REFERENCES

Abas, N., Kalair, A., & Khan, N. (2015). Review of Fossil Fuels and Future Energy Technologies. *Futures, 69*, 31–49.

Aryadi, W., Valentino, M. P. J., & Apriaskar, E. (2025). Performance Analysis of 18-Slot 12-Pole Ring-Type Orbital Electric Motor with Variations of Neodymium and Low-Carbon Steel Rotors Using FEMM 4.2 Software. *Rekayasa, 23*(1), 41–56.

Azizi, M. F., Hadi, W., & Kalandro, G. D. (2020). Rancang Bangun Motor BLDC Axial Flux Menggunakan Dua Kawat Email pada Lilitan Kumparan Stator. *Jurnal Arus Elektro Indonesia, 6*(2), 52–57.

Choudhary, A., Goyal, D., Shimi, S. L., & Akula, A. (2019). Condition Monitoring and Fault Diagnosis of Induction Motors: A Review. *Archives of Computational Methods in Engineering, 26*(4), 1221–1238.

Dermani, M. K. (2025). *Modelling of Electromagnetic Couplings by a Systemic Approach for the Energy Efficiency of Static Converters* [Doctoral dissertation, Université de Toulouse].

Dusane, P. M. (2016). *Simulation of a Brushless DC Motor in ANSYS-Maxwell 3D* [Master's thesis, Czech Technical University in Prague].

Ehya, H., Skreien, T. N., & Nysveen, A. (2021). Intelligent Data-Driven Diagnosis of Incipient Interturn Short Circuit Fault in Field Winding of Salient Pole Synchronous Generators. *IEEE Transactions on Industrial Informatics, 18*(5), 3286–3294.

Fitrianto, H. (2023). Analisis Penggunaan Kendaraan Listrik sebagai Upaya Penurunan Emisi Lingkungan (Case Study Kendaraan Listrik di Provinsi Sumatera Utara). *Cakrawala Repositori IMWI, 6*(2), 1056–1067.

Gecer, B., Fusun, N., & Serteller, N. F. O. (2020). Understanding Switched Reluctance Motor Analysis Using ANSYS/Maxwell. *2020 IEEE 29th International Symposium on Industrial Electronics (ISIE)*, 446–449.

Guo, J., Zhao, Q., & Xi, M. (2022). Sustainable Urban Logistics Distribution Network Planning with Carbon Tax. *Sustainability, 14*(20), 13184.

Hao, W., Hao, J., Wang, Z., & Hao, Y. (2022). Decoupling Characteristics and Torque Analytical Model of Sharing-Suspension-Windings Bearingless Switched Reluctance Motor Considering Flux-Linkage Saturation. *Sustainability, 14*(24), 16633.

Hashemnia, N., & Asaei, B. (2008). Comparative Study of Using Different Electric Motors in the Electric Vehicles. *2008 18th International Conference on Electrical Machines*, 1–5.

Islam, Z., Khan, F., Ullah, B., Milyani, A. H., & Azhari, A. A. (2022). Design and Analysis of Three Phase Axial Flux Permanent Magnet Machine with Different PM Shapes for Electric Vehicles. *Energies, 15*(20), 7533.

Jin, S., Liu, N., & Ma, C. (2024). Quantum Simulation of Maxwell's Equations via Schrödingerisation. *ESAIM: Mathematical Modelling and Numerical Analysis, 58*(5), 1853–1879.

Kahar, M. I., Othman, R. N. F. K. R., Khamis, A., Abdullah, N., Shukor, F. A. A., & Tat, L. S. (2022). Effect of Slot-Pole Numbers on the Performance of a BLDC Motor for Agro-EV Application. *ECTI Transactions on Electrical Engineering, Electronics, and Communications, 20*(1), 51–61.

Khan-Ngern, W., Keyoonwong, W., Chatsiriwech, N., Sangnopparat, P., Mattayaboon, P., & Worawalai, P. (2018). High-Performance BLDC Motor Control for Electric Vehicle. *2018 International Conference on Engineering, Applied Sciences, and Technology (ICEAST)*, 1–4.

Kuczmann, M. (2024). Review of DC Motor Modeling and Linear Control: Theory with Laboratory Tests. *Electronics, 13*(11), 2225.

Liu, Z., Zhang, G., & Du, G. (2024). An Investigation into the Pole–Slot Ratio and Optimization of a Low-Speed and High-Torque Permanent Magnet Motor. *Applied Sciences, 14*(10), 3983.

Madras Ponnuswamy, V., & Veeranna, S. B. (2026). Efficiency and Loss Analysis of Circular, Square and Round-Cornered Square Coils in Wireless Power Transfer System—A Comparative Study Using Ansys Maxwell 3D. *World Electric Vehicle Journal, 17*(7), 364.

Mei, L., Xiao, W., Cui, J., Zhang, Q., & Liu, Z. (2023). Analytical Modeling and Pole–Slot Combination Selection Analysis of a Direct-Drive Drilling Permanent Magnet Synchronous Motor. *Processes, 11*(11), 3222.

Mohanraj, D., Aruldavid, R., Verma, R., Sathiyasekar, K., Barnawi, A. B., Chokkalingam, B., & Mihet-Popa, L. (2022). A Review of BLDC Motor: State of Art, Advanced Control Techniques, and Applications. *IEEE Access, 10*, 54833–54869.

Muljono, A. B., Dharma, I. B. A. L., & Citarsa, I. B. F. (2025). Pengaruh Pembebanan Transformator Distribusi 3 Fasa 250 kVA Type Core terhadap Distribusi Termal Menggunakan Perangkat Lunak Ansys Maxwell. *DIELEKTRIKA, 12*(2), 38–47.

Pliuhin, V., Petrenko, O., Tsegelnyk, Y., Duniev, O., Yehorov, A., & Khudiakov, I. (2022). Optimization of Electromechanical Energy Converters With a Solid Rotor Output Parameters in ANSYS RMxprt. *Lighting Engineering & Power Engineering, 61*(3), 74–85.

Sofaniadi, S., Huda, M., & Hartawan, F. (2022). Transportasi Berkelanjutan dan Pengaruhnya terhadap Pengurangan Emisi di Kota Semarang. *Jurnal Riptek, 16*(1), 81–89.

Sofwatillah, Risnita, Jailani, M. S., & Saksitha, D. A. (2024). Tehnik Analisis Data Kuantitatif dan Kualitatif dalam Penelitian Ilmiah. *Jurnal Genta Mulia, 15*(2), 79–91.

Sudjoko, C. (2021). Strategi Pemanfaatan Kendaraan Listrik Berkelanjutan sebagai Solusi untuk Mengurangi Emisi Karbon. *Jurnal Paradigma: Jurnal Multidisipliner Mahasiswa Pascasarjana Indonesia, 2*(2).

Tjong, W. F. (2021). *Pengantar Metode Elemen Hingga untuk Analisis Struktur: Teori, Perumusan, Implementasi Komputer, dan Aplikasi.* Rajawali Pers.